Materials Today Bio 29 (2024) 101338

Contents lists available at ScienceDirect

Materials Today Bio

journal homepage: www.journals.elsevier.com/materials-today-bio

Harnessing hydrogen sulfide in injectable hydrogels that guide the immune response and osteoclastogenesis balance for osteoporosis treatment

Lianghua Jiang [a,1], Yubin Wu [b,1], Zonghan Xu [c,1], Mingzhuang Hou [b], Shayang Chen [a], Chao Cheng [a], Dan Hu [c,*], Daming Lu [a,**], Xuesong Zhu [b,***], Chong Li [a,****]

[a] Department of Orthopedics, Affiliated Kunshan Hospital of Jiangsu University, Jiangsu, 215300, China
[b] Department of Orthopaedics, The First Affiliated Hospital of Soochow University, Suzhou, 215006, Jiangsu, China
[c] Department of Orthopedics, The Affiliated Suzhou Hospital of Nanjing Medical University, Suzhou Municipal Hospital, Gusu School of Nanjing Medical University, Suzhou, 215008, China

ARTICLE INFO

Keywords:
Osteoporosis
H_2S-Releasing hydrogel
ROS-Responsive
Inflammatory
Bone regeneration

ABSTRACT

Elevated levels of oxidative stress, inflammation, and a dysregulated osteoclastogenesis balance frequently characterize the microenvironment of osteoporosis, which impedes the processes of healing and repair. Existing treatment approaches are limited in scope and rely primarily on factors and drugs. An injectable hydrogel designed for the ROS-responsive release of H_2S gas is presented in this study. The first network of the hydrogel comprises sodium alginate (SA-SATO) chelated with S-aroylthiooxime (SATO) and an H_2S-generating group, while the second network is composed of photocrosslinkable PEGDA. Through the integration of Cys-releasing microspheres that are reactive with ROS, a composite hydrogel was developed that exhibited advantageous mechanical characteristics and biosafety. The composite hydrogel effectively promoted osteogenic differentiation of mesenchymal stem cells, modulated macrophage polarization, decreased inflammatory responses, and halted cell apoptosis, as evidenced by in vitro experiments. Additionally, it released H_2S gas and mitigated excess ROS in cells. The efficacy of the composite hydrogel in promoting bone defect repair and regeneration in an osteoporotic model was further validated by in vivo findings. In summary, the composite hydrogel exhibits potential as a viable approach to address osteoporotic bone defects by harmonizing osteogenesis and osteoclast activity, modulating the microenvironment of bone injuries, and reducing inflammation. Consequently, it presents a viable strategy for the efficient repair of bone defects.

1. Introduction

Osteoporosis and other age-related skeletal diseases are distinguished by diminished bone mass and a compromised microstructure of bone tissue [1]. These factors contribute to heightened bone fragility, porosity, and susceptibility to fractures, which substantially impede the repair of bone fractures and defects in osteoporotic patients [2]. Bone grafting is a frequently utilized technique in the treatment of osteoporotic defects [3]. Although autologous bone transplantation has demonstrated favorable clinical results, it is constrained by the availability of donor sites and carries the risk of additional patient trauma. As a result, the development of novel biomaterials capable of promoting osteoporotic bone regeneration must be a top priority. Because allogeneic and xenograft bone transplantation carry the potential hazards of immunogenicity and disease transmission, this is of the utmost importance. An environment characterized by bone loosening is characterized by elevated levels of oxidative stress [4], inflammation, and osteoclast-osteoblast imbalance [5]. An increase in the activity of osteoclasts causes excessive bone resorption, whereas a decrease in the activity of osteoblasts reduces the rate of bone formation [6,7]. To promote bone repair in such an environment, it is therefore essential to reduce oxidative stress and the inflammatory microenvironment

* Corresponding author.
** Corresponding author.
*** Corresponding author.
**** Corresponding author.
E-mail addresses: 13962109088@163.com (D. Hu), ludamingks@163.com (D. Lu), zhuxs@suda.edu.cn (X. Zhu), lichong1705@163.com (C. Li).
[1] These authors contributed equally to this work.

https://doi.org/10.1016/j.mtbio.2024.101338
Received 20 July 2024; Received in revised form 28 October 2024; Accepted 10 November 2024
Available online 12 November 2024

associated with bone resorption, inhibit osteoclast formation, and restore the viability of stem cells and osteoblasts.

Hydrogen sulfide (H_2S) is a gas transmitter that functions as a cellular messenger molecule in the human body. It has garnered significant attention due to its various physiological and pathophysiological roles in different systems [8,9]. Endogenous H_2S is generated via the action of cysteine sulfide β-synthases (CBSs) and cysteine sulfide γ-lyase (CSE), which facilitate the synthesis of cysteine and homocysteine [10–12]. The vascular system, heart, kidney, brain, nervous system, lower gastrointestinal tract, skeletal muscle, and bones all contain these enzymes [13]. The therapeutic potential of H_2S for a wide range of diseases has garnered biomedical scientists' growing interest. Recent research has unveiled its participation in the process of bone repair, thereby suggesting its potential as a regulator of bone formation. It has been demonstrated that H_2S preserves the stemness and functionality of mesenchymal stem cells in bone marrow, thereby promoting osteoblast survival in an environment of bone loosening. A multitude of H_2S prodrugs have been the subject of investigation in clinical or preclinical trials in recent years [14]. Despite this, the precise mechanism of action and method of regulating the release of H_2S in vivo remain unknown. To investigate the effect of H_2S on bone defect repair in the context of bone loosening, it is necessary to develop an H_2S release system that can be controlled.

In recent years, there has been considerable attention directed towards hydrogels on account of their bionic three-dimensional polymer network structure, exceptional mechanical properties, rheological behavior, and biocompatibility [15]. By functioning as carriers, they have the ability to encapsulate S-aroylthiooxime (SATO), a thiol-responsive donor of H_2S [16]. This facilitates the regulated release of H_2S, improves operational effectiveness, and mitigates the inadvertent release and leakage of loaded H_2S donors, thus diminishing the likelihood of adverse effects. Sodium alginate, which is readily available and inexpensive, is a prevalent natural macromolecular substance composed primarily of the compounds -L-guluronic acid (G) and β-D-mannuronic acid (M) [17,18]. By selectively oxidizing periodate salts, sodium alginate can be converted into a variety of polysaccharide derivatives, including alginate dialdehyde (ADA) [18]. Sodium alginate is abundant in coordination and reaction sites, respectively, carboxyl (-COOH) and hydroxyl (-OH) groups [19]. The preparation of the sodium alginate/Ca^{2+} gel network is straightforward and widely recognized [20,21]. Nevertheless, the expeditious and uneven amalgamation of calcium ions and sodium alginate may impede the preparation of injectable hydrogels, necessitating the implementation of an additional network for this purpose. Good biocompatibility characterizes the hydrophilic polyethylene glycol diacrylate (PEGDA) [22,23]. Its terminal double bonds are capable of reacting to form a gel network; when combined with natural polymers, they frequently produce a double network gel with enhanced mechanical strength. We prepared injectable hydrogels with responsive H_2S release in order to target the inflammatory microenvironment within the osteoporotic environment in this study. Our objectives were to decrease the formation of osteoclasts, restore the function of osteoblasts, and facilitate the repair of defects in the osteoporotic environment.

2. Materials and methods

2.1. Materials

Sodium alginate, Sodium periodate, hydroxylamine-O-sulfonate, thiobenzoic acid, PVA (1788) and PEGDA (Mn = 1000) was purchased from Aladdin. N,N,N′,N' -tetramethyl-1,3-propanediamine, 4-(bromomethyl) phenylboronic acid and lithium acylphosphinate salt (LAP) were from Sigma-Aldrich (Shanghai, China). Fetal bovine serum (FBS), phosphate-buffered saline (PBS), a-minimum essential medium (α-MEM), and dulbecco's modified eagle medium (DMEM) were purchased from Gibco (Grand Island, NY, USA). The antibodies (CD31, α-SMA, Col I) were purchased from Abcam. The antibodies CD86, CD206) were purchased from BD.

2.2. Synthesis of S-benzoylthiohydroxylamine (SBTHA) and oxidized alginate (SA-CHO)

SBTHA was synthesized as reported before [24]. To synthesize SBTHA, hydroxylamine-O-sulfonate (1.13 g) was dissolved in 10 mL of 1M NaOH in an ice bath to create a 1M hydroxylamine- O- sulfonate sodium solution. Next, thiobenzoic acid (1.11 g, 8 mmol) was dissolved in 16 mL of 0.5M NaOH to form a 0.5M sodium thiobenzoate solution. Then, sodium hydroxylamine-O-sulfonate was slowly added dropwise to the thiobenzoate solution in an ice bath and stirred for 30 min. The resulting white precipitate was collected by filtration and washed with water, followed by freeze-drying for future use.

Oxidized alginate (SA-CHO) was synthesized as reported before [25]. A mixture of sodium alginate solution (5.00 g in 450 mL distilled water) and sodium periodate aqueous solution (5.40 g in 50 mL distilled water) should be prepared and stirred. The reaction should take place at room temperature in the dark for 24 h. Once the reaction is complete, ethylene glycol (3.00 mL) should be added and stirred for 0.5 h to stop the reaction. The resulting product should then be transferred into a 7000 kDa dialysis bag for purification through dialysis. Finally, freeze-drying should be performed to obtain the SA-CHO product.

2.3. Conjugation of SBTHA to SA-CHO (SA-SATO)

In order to prepare H2S releasing gel, SBTHA was first grafted onto aldehyde-containing SA-CHO to synthesize SA-SATO polymer. Briefly, for preparation SA-SATO polymer, 1.0g SA-CHO was dissolved in 100 mL ultrapure water. Then, SBTHA (10 eq. corresponding to aldehyde group) was added and dissolved. The reaction mixture was shaken at 25 °C for 12 h over molecular sieves, and subsequently transferred to dialysis bag for dialysis purification. Finally, product obtained after freeze-drying.

2.4. Preparation of ROS-responsive microparticles containing cysteine (Cys)

The ROS-responsive microparticles was from the ROS-responsive hydrogel. The hydrogel was prepared through reaction between phenylboronic acid existing in TPA (ROS-labile linker) and alcohol hydroxyl groups from PVA by simply mixing 50 mg TPA and 50 mg PVA. ROS-responsive crossslinker (N-(4-boronobenzyl)-N′-(4-boronophenyl)- N, N, N′, N′-tetramethylpropane-1,3-diaminium,TPA) was synthesized via quaternization reaction of N, N, N′, N′-tetramethyl-1,3-propanediamine and 4-(bromomethyl) phenylboronic acid was synthesized as reported before [26]. In order to prepare micro particles, gel is placed in a grinder and crushed under the cooling of liquid nitrogen to obtain.

2.5. Preparation of PEGDA/SA-SATO-Ca composite (PESATO/MCys-Ca) hydrogel

The double network hydrogel is created through a combination of free radical polymerization and ionic bonding of PEGDA and a polymer chain that includes H_2S. To begin, a 40 % (w/v) PEGDA aqueous solution, 5 % SA-SATO aqueous solution, and a mixture of 15 mg/mL LAP and 100uM $CaCl_2$ solution in a 1:1:1 vol ratio are prepared. Subsequently, crosslinking is induced under blue light to form a gel. In the preparation of PESATO/MCys-Ca, 200 mg microparticles containing Cys are encapsulated within the 1 mL PESATO hydrogel. Upon release from the microparticles, the mercaptan-containing compound cysteine (Cys) diffuses into the gel, resulting in the generation of H_2S. The morphology and shape of hhydrogels were examined via scanning electron microscopy (SEM, Hitachi S-4800, Japan). The compression behavior of the hydrogel was evaluated by a commercial mechanical tensile machine

(AG-2000A, Shimadzu, Japan).

For test of H_2S Release in the Presence of Cysteine, H_2S release was measured using a modified methylene blue colorimetric assay as previously reported [27,28]. Place 200 mg of gel in 2 mL of solution containing 2 mM $Zn(OAc)_2$ and 1 mM cysteine solution, and take 100 out of each vial at a predetermined time point μ L. Every 100 μ Use 100 for L equal parts of the sample μ Dilute with L $FeCl_3$ solution (30 mM in 1.2M HCl) and then use 100 μ Dilute L N, N-dimethyl-p-phenylenediamine (20 mM in 7.2M HCl). After taking the last aliquot, store the aliquot for at least 24 h. Measure the absorbance of each sample at 750 nm using a flat panel reader. Perform kinetic analysis by subtracting the absorbance of the blank solution from the average absorbance at each time point.

2.6. Cell culture

The bone marrow mesenchymal stem cells (BMSCs) were harvested from the femora and tibias of four-week-old Sprague-Dawley (SD) rats and cultured in α-MEM medium supplemented with 10 % FBS and 1 % of penicillin/streptomycin in a humidified incubator (37 °C and 5 % CO_2). The adherent cells were cultured and passaged when they reached 80–90 % confluence. The Passage 3 BMSCs were used in this study.

For the acquisition of the bone marrow mononuclear cells (BMMs), bilateral tibias and femurs of 8-week-old C57BL/6 mice were obtained, and the bone marrow cavity was thoroughly rinsed with a-MEM. After centrifugation at 1200r/min for 5 min, the supernatant was discarded. The bottom cells were lysed with sterile red blood cell lysis solution on ice for 5 min, and after centrifugation at 1200r/min for 5 min, the supernatant was discarded. The cells were resuspended and placed in a culture bottle. After 1 day, the supernatant cells were collected and cultured with 50 ng/ml M-CSF for 3 days. The adherent cells were mononuclear macrophage BMMs.

The murine-derived macrophage cell line RAW 264.7 and HUVECs used in this study were from Shanghai Institutes for Biological Science. The cells were cultured in DMEM medium supplemented with 10 % FBS and 1 % of penicillin/streptomycin in a humidified incubator (37 °C and 5 % CO2).

2.7. Ability of the hydrogel to scavenge intracellular ROS

The excessive ROS can lead to non-union of bone tissue and exacerbate the inflammatory response [29]. The intracellular ROS-scavenging activity of hydrogel was evaluated through a ROS indicator 2',7'- dichlorodihydrofluorescein diacetate (DCFH-DA). Briefly, RAW264.7 (2×10^4 cells/well) were seeded in a 24-well plate and cultured with different treatment for 24 h 100 ng/mL LPS was added to initiate excess oxidative stress. Then, cells were washed and incubated with 10 μM DCFH-DA at 37 °C for 1 h. After that, flow cytometry was conducted on a Flow Cytometer BD Fortessa X-20 (BD Biosciences), and results were further analyzed with the FlowJo software (FlowJo, LLC) and fluorescence images were captured by confocal microscope (Nikon, Japan).

2.8. Assessment of macrophage polarization

The bone tissues of patients with osteoporosis exhibit chronic inflammation, which leads to an increase in the pro-inflammatory M1 macrophages. Therefore, the M1 polarization of macrophages under different treatments was investigated. The polarization effect of hydrogel system on macrophages was assessed using flow cytometry. RAW264.7 cells were treated with either LPS (100 ng/mL) or hydrogel cocultured through Transwell for 24 h. Subsequently, the cells were detached using a cell scraper, blocked with CD16/32 for 10 min, and then stained with CD86 and CD206 antibodies for 30 min. Following centrifugation, the cells were resuspended and analyzed using a flow cytometer.

2.9. Osteoclast culture assay

For the induction and culture of osteoclasts, bone marrow macrophages (BMMs) are scraped off when the fusion degree reaches 80–90 % and plated in a 12-well plate at a density of 2x10^5 cells/well. The cells are then cultured in alpha-minimum essential medium (a-MEM) containing 330 ng/ml M-CSF until the fusion degree reaches 80–90 %, after which 50 ng/mL of RANKL factor is added to induce osteoclast formation. The following day, the culture medium with the inducing factor is changed to observe cell morphology. After 5–6 days, large irregular multinucleated osteoclasts fused with multiple monocytes can be observed under a microscope. In the co-culture of osteoblasts and osteoclasts, osteoclasts treated differently are seeded at the bottom using Transwell, while osteoblasts are placed in small chambers. The morphology of osteoclasts is observed, and the secretion of RANKL and OPG factors in the medium is tested using ELISA. Subsequently, TRAP staining is performed using the Sigma Aldrich white blood cell acid phosphatase kit following the manufacturer's instructions. TRAP positive multinucleated cells with 3 or more nuclei are identified as osteoclasts. Osteoclasts are then observed under a microscope, photographed, and quantified.

2.10. Cytotoxicity and cell proliferation of hydrogel

The cytotoxicity of various gels was assessed using the CCK-8 method. Bone marrow mesenchymal stem cells ($2 \times 10^4 mL^{-1}$) were seeded into each well of a 24-well plate. After cell adhesion, the gels were co-cultured for 1 and 4 days using a transwell system. CCK-8 solution was added to each well at the specified time points, and the cells were then incubated in a 5 % carbon dioxide incubator at 37 °C for 1 h. Subsequently, 100 μL of the solution was transferred to a 96-well plate and the absorbance at 450 nm was measured using an enzyme-linked immunosorbent assay (ELISA) reader.

2.11. Osteogenic induction and evaluation

Passage 3 BMSCs were seeded on 24-well plate as 2×10^4 under different treatment through Transwell. An alkaline phosphatase (ALP) activity assay and Alizarin Red S (ARS) staining and quantification were used to evaluate osteogenic differentiation. BMSCs were cultured in osteogenic induction media with varying components for 3 and 7 days, followed by fixation with 4 % paraformaldehyde and staining for ALP. Stained images were captured using a microscope. For ARS staining, BMSCs were cultured in osteogenic induction media with different components for 7 and 14 days, fixed with 4 % paraformaldehyde, and then incubated with 0.1 % ARS solution (pH = 4.8) for 30 min. Subsequently, the excess dye was removed by washing the samples with ultrapure water, and calcium nodules were observed under a microscope.

2.12. Tube formation assay

Human umbilical vein endothelial cells (HUVECs) were utilized in a tube formation assay to examine the effects of various treatments. Initially, the HUVECs were pre-treated with different gels for a period of 3 days. Subsequently, 200 μL of matrix gel was added to a pre-cooled 48-well plate and placed in an incubator. Following this, 10×10^4 treated HUVECs were seeded onto the matrix gel and allowed to incubate for 6 and 12 h. Tube formation was then assessed under a microscope, and each group was quantified using ImageJ software.

2.13. Quantitative real-time polymerase chain reaction (qRT-PCR) analysist

BMSCs were treated with H_2O_2 (100 μM) and cocultured with different hydrogels by transwell assay in 6-well plates. After 48 h of culture, the culture medium was absorbed and washed twice with PBS,

and the total RNA of the cells was extracted with Trizol reagent. Real time quantitative polymerase chain reaction (qRT-PCR) was performed to determine the mRNA expression. GAPDH served as a housekeeping gene.

2.14. Establishment of osteoporotic bone defect model and implantation of hydrogels

All animal treatment procedures are carried out in accordance with the guidelines of the Animal Care Committee of Soochow hospital. SD rats (female, 200 ± 20 g) were purchased from the Experimental Animal Center of Soochow hospital. Osteoporosis models were induced through bilateral oophorectomy (OVX), with sham surgery performed on the sham group, as previously documented [30]. Following anesthesia with intraperitoneal injection of sodium pentobarbital (30 mg/kg) under sterile conditions, the rats were disinfected with iodine solution and medicinal alcohol, and positioned in a prone position. Subsequently, a dorsal incision was made to remove both ovaries and ligate the fallopian tubes. The rat model of osteoporosis was confirmed using micro CT at one and two months post-surgery. Once the osteoporosis model was established, the rats were randomly allocated into four groups: Sham and OVX groups as the control groups, and different hydrogels were implanted in the experimental group simultaneously. A 1 cm diagonal incision was made on the inner skin of the distal femoral joint to expose the bone by separating the fascia and muscles directly. A 3 mm surgical drill bit was used to create a deep non-penetrating defect 4 mm below the cartilage growth plate perpendicular to the bone surface. The cavity defects in the experimental group were filled with composite gel. Post-operatively, penicillin was administered at a standard dose of 800, 000 units per day for 3 days. Rats were euthanized at 4 and 8 weeks after surgery, and their femurs were extracted for further analysis.

2.15. Micro-CT analysis

To evaluate the quality of new bone formation, we collected femurs with defect areas for Micro CT imaging at weeks 4 and 8 after stent implantation. Micro-computed tomography (micro-CT) was performed to scan the skull defects using SkyScan under a standard condition (40 kV X-ray voltage; 250 μA electric current; 18 μm per pixel). Three-dimensional (3D) images of micro-CT were reconstructed using Data-Viewer (version 1.5.1.2, Bruker, Kontich, Belgium). A diameter of 3 mm that covered the bone defect region in reconstructed 3D images was defined as the region of interest (ROI).

2.16. Histological examination

In order to further evaluate the osteogenesis of hydrogel, samples were stained with hematoxylin and eosin (H&E), Masson, TRAP, immunohistochemistry (IHC) and immunofluorescence. At the scheduled time (4 and 8 weeks), the animals were euthanized and the harvested femur was fixed with 4 % paraformaldehyde. Then, use 15 % EDTA to decalcify the femur until it can be embedded and sliced. After embedding through gradient dehydration, the wax blocks were cut into 4.5 μm sections for staining. For IHC, the osteogenic marker collogen 1 (Col I) and angiogenesis marker (CD31) were selected for staining. Soak the slices in a 3 % hydrogen peroxide solution for 15 min and clean them three times. Then use sodium citrate antigen repair solution and microwave method for antigen repair. After cleaning, block the sections with 10 % goat serum. After removing the blocking solution and washing, incubate overnight with primary antibody CD31(abcam, USA) or Col I (abcam, USA). Then, the processed slices were incubated with secondary antibody working solution and corresponding horseradish peroxidase (HRP) coupled streptomycin working solution at 37 °C. Then drop the substrate solution of 3-3 ′- diaminobenzidine onto the slice. When brown positive particles appear in the target tissue but no specific color appears in the surrounding tissue, distilled water is added to prevent color development. In order to investigate the ability to form blood vessels, immunofluorescence staining was used to observe the formation of capillaries (CD31 positive) and mature blood vessels (a-SMA positive) around the defect.

2.17. Statistical analysis

Statistical analysis was conducted with GraphPad Prism Software (GraphPad Software Inc.), and all the numerical results were presented as mean ± standard deviation. One-way ANOVA was used to examine group differences. Statistical significance was defined as $*p < 0.05$, while $**p < 0.01$indicated extreme significance.

3. Results and discussion

3.1. Preparation and characterization of PESATO/MCys-Ca

As shown in Fig. 1, we fabricated an injectable dual network gel responsive to H_2S release and an SA-SATO polymer chain that releases H_2S via the formation of SATO. Cys diffuses into the PESATO hydrogel network when microparticles are present in the microenvironment of osteoporosis, which is characterized by elevated oxidative stress. SATO exhibits a specific response to mercaptan-containing compounds, releasing H_2S. The FT-IR spectra of SA and SA-CHO exhibited a broad band at 3185 cm^{-1}, which corresponds to the OH groups, as illustrated in Fig. 2A. The bands at 1686 and 1528 cm^{-1} were identified as aromatic C=C groups. The medium band at 1528 cm^{-1} was indicative of carboxylate salt ions. The band at 752 cm^{-1} was indicative of benzene rings that were ortho-1,2-substituted. The FT-IR spectrum of SA-CHO revealed the presence of a new absorption band at 1736 cm^{-1}, which corresponded to the stretching vibration of the C=O group on the carbonyl groups of the aldehyde. This finding confirmed the successful synthesis of SA-CHO. The FT-IR analysis of SBTHA and SA-SATO revealed that subsequent to the conjugation of SATO, the peak at 1736 cm^{-1} vanished and a new peak at 1683 cm^{-1} materialized, which corresponds to the stretching vibration of the thiooxime C=N bond. This discovery is consistent with results that have been previously reported [31].

The results of the vial inversion test (Fig. 2B) demonstrated that gels comprising various components can form rapidly and display fluidity prior to solidifying, thereby establishing injectability. Tthe particles extracted from the ROS-responsive gel are on the micron scale (Fig. 2C). The porous structures of both the PESATO hydrogel and the PESATO/MCys-Ca gel are evident from the SEM images, as depicted in Fig. 2C. As illustrated in Fig. 2D–F, the PESATO/MCys-Ca gel recovers from compression and possesses a greater compressive modulus. PESATO hydrogel degraded more slowly than PESATO/MCys-Ca gel under oxidative stress (100 μM H_2O_2) (Fig. 2G). As depicted in Fig. 2H, the PESATO/MCys-Ca gel released H_2S for a duration of seven days when Cys was present. This finding suggests that the gel possesses the capability to be utilized in long-term therapeutic applications. Nevertheless, when Cys was absent, the release of H_2S was virtually undetectable, suggesting that SATO is particularly sensitive to compounds containing thiols.

3.2. ROS levels in RAW264.7 cells after different interventions

High levels of oxidative stress and osteoclast activity characterize the microenvironment of osteoporosis; these factors can inhibit osteogenic activity and have an effect on the repair of bone defects [32,33]. By decreasing intracellular reactive oxygen species (ROS) production, H_2S can prevent oxidative damage induced by hydrogen peroxide, thus promoting epidermis tissue repair [34]. Thus, we conducted an investigation into the ROS removal capability of the hydrogels. LPS increased ROS production in RAW264.7 cells, as demonstrated in vitro; this underscores the significance of materials possessing antioxidant properties

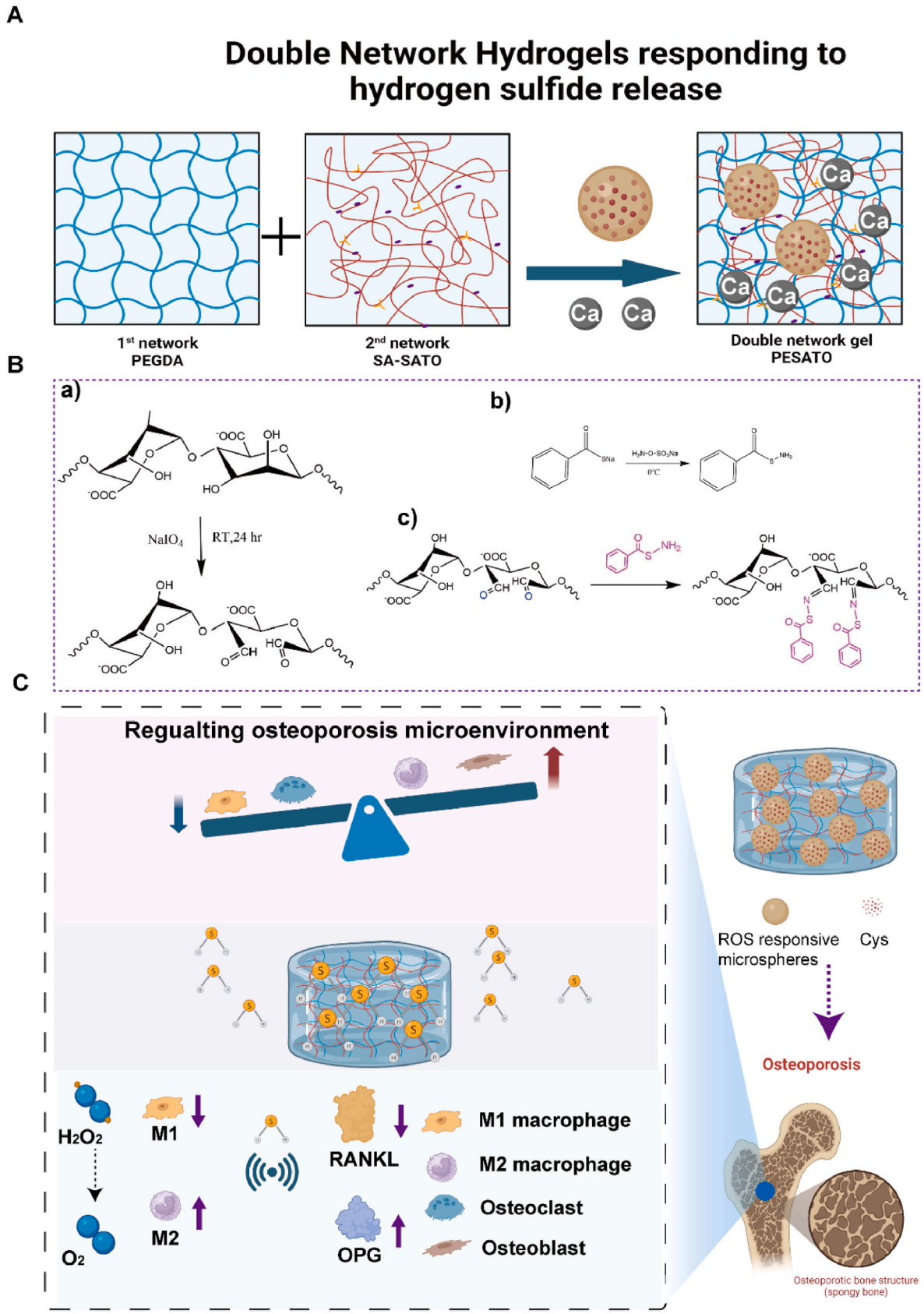

Fig. 1. Schematic diagram of design and preparation of composite PESATO/MCys-Ca injectable hydrogel which can slow release hydrogen sulfide gas and respond to ROS microenvironment. PESATO/MCys-Ca injectable hydrogels can guide the immune response and osteoclastogenesis balance for osteoporosis rreatment.

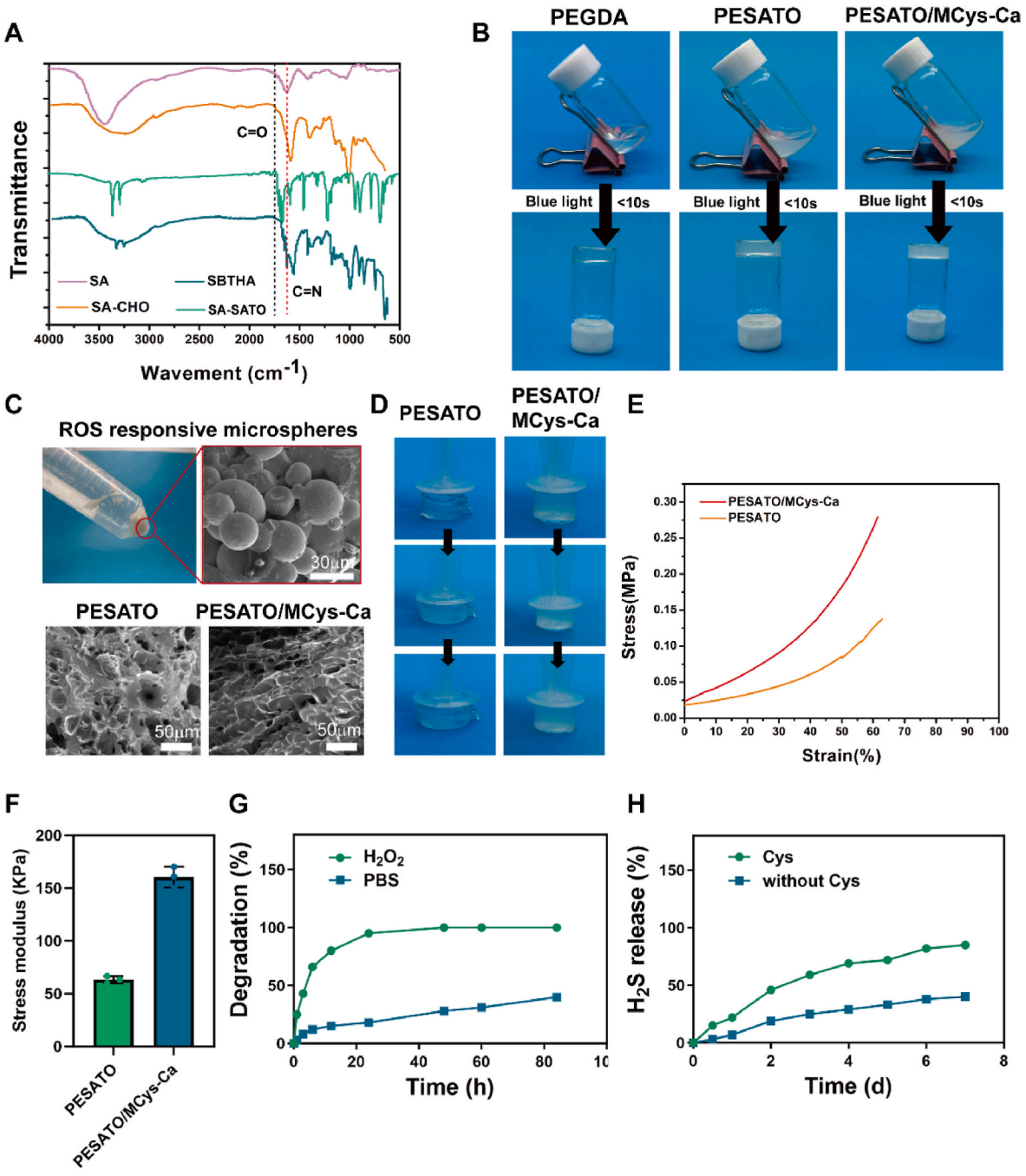

Fig. 2. Synthesis and characterization of composite hydrogel for repairing osteoporotic bone defect and releasing hydrogen sulfide gas. (A) FTIR spectroscopy of SA, SA-CHO, SBTHA and SA-STAO. (B) Gelation photos of different hydrogel. (C) SEM images of microspheres and hydrogels. (D) Compressive appearance of hydrogel. (E) Compression curve of hydrogel. (F) Stress modulus of different hydrogel. (G) Degradation of PESATO/MCys-Ca hydrogel with or without H_2O_2. (H) H_2S releasing curves of PESATO/MCys-Ca in the presence of Cys.

in the treatment of osteoporotic bone defects. As illustrated in Fig. 3A, the average cellular ROS concentration in the LPS-treated RAW264.7 cells exhibited a substantial increase in time when compared to the control group. However, the application of PESATO/MCys-Ca treatment significantly reduced the intensity of ROS. Furthermore, the intracellular ROS fluorescence images (Fig. 3B) exhibited a comparable phenomenon. Clearly, these effects were mitigated through the application of PESATO/MCys-Ca. According to these findings, PESATO/MCys-Ca exhibited potent antioxidant properties.

3.3. Anti-inflammatory characteristics of PESATO/MCys-Ca

Successful regeneration in osteoporotic bone defects necessitates the establishment of a favorable microenvironment and the regulation of the immune inflammatory response; these aspects comprise a multidimensional management process. Controllable H_2S exerts anti-inflammatory properties [35]. In regions where bone resorption defects are present, macrophages commonly exhibit a proinflammatory M1 phenotype, which has the potential to hinder the healing process. In order to examine the potential anti-inflammatory attributes of the hydrogels, we conducted an assay to determine the effect of various materials on the polarization of RAW264.7 cells in the direction of the M1 phenotype. By

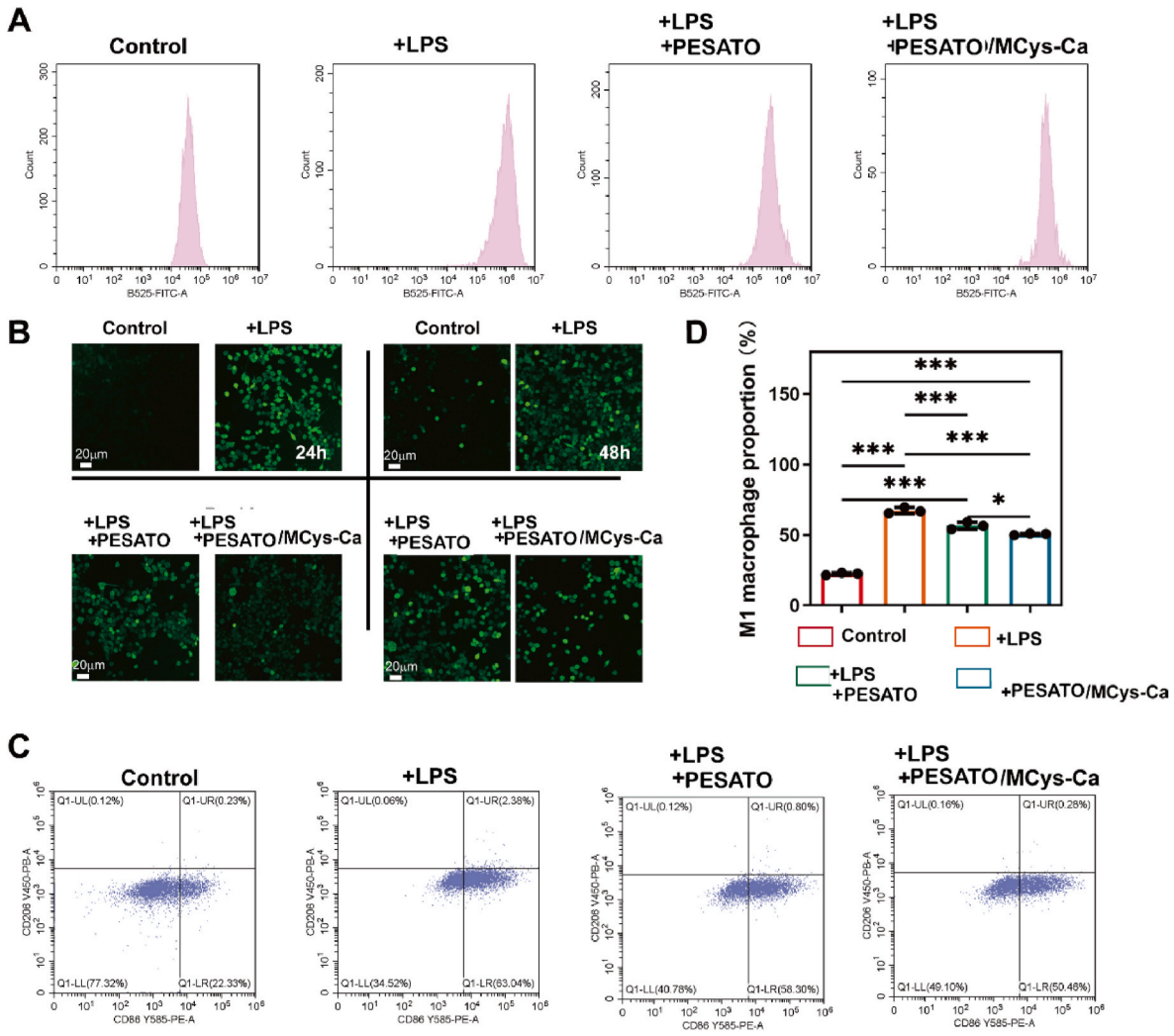

Fig. 3. Antioxidant and anti-inflammatory properties of composite hydrogels. (A) Intracellular ROS detection of RAW264.7 cells detected by flow cytometry. (B) Representative fluorescence images of cellular ROS under different treatments. Scale bars: 100 μm. (C–D) Evaluation of M1 polarization of RAW264.7 cells by flow cytometry under different treatments.

utilizing flow cytometry, the surface markers of RAW264.7 cells that had undergone diverse treatments were analyzed. Concurrently detecting the anti-inflammatory cytokine CD206 and the proinflammatory marker CD86 allowed for the evaluation of the polarization of RAW264.7 cells. As illustrated in Fig. 3C–D, LPS induced an inflammatory response; consequently, in the absence of material treatment, there were significantly more CD86-positive cells than CD206-positive cells. Following treatment with the hydrogels, the number of CD86-positive cells decreased. Furthermore, the most conspicuous reduction was noted in the group treated with PESATO/MCys-Ca. Nevertheless, there was no increase in the quantity of CD206-positive cells in response to the hydrogels. The potent antioxidant properties of the released H_2S may account for this. According to these findings, PESATO/MCys-Ca is capable of efficiently inhibiting the inflammatory response, thereby ameliorating the severe inflammatory microenvironment associated with osteoporotic bone defects.

3.4. *PESATO/MCys-Ca inhibits osteoclastogenesis in vitro*

The investigation employed tartrate-resistant acid phosphatase (TRAP) and F-actin staining techniques to assess the impact of various gel formulations on the generation of osteoclasts (Fig. 4A–D). When RANKL was introduced, osteoclasts were effectively generated, and osteoclast formation was superior to that of the control group. Nonetheless, osteoclast formation was diminished subsequent to induction coculture with gel, and this reduction was particularly pronounced in the PESATO/MCys-Ca group. The findings suggest that the negative regulation of osteoclast generation through the emission of a substantial quantity of H_2S can be elucidated by the formation of osteoclasts within mononuclear macrophages treated with PESATO/MCys-Ca.

Osteoblasts facilitate bone resorption and osteoclast development during the normal phase of bone remodeling through the secretion of RANKL. Additionally, osteoclasts secrete OPG, which further enhances osteoblast vitality and promotes bone regeneration. Osteogenesis and osteoclasts are frequently unbalanced in the microenvironment of osteoporosis, which can impede bone repair [36,37]. In order to ascertain the potential impact of gel treatment on osteoblast activity, coculture experiments were performed involving preosteoblasts and osteoclasts (Fig. 4E). First, RANKL and OPG concentrations in the supernatant of the coculture system were determined. As shown in Fig. 4F–G, the PESATO/MCys-Ca group secreted a greater quantity of OPG but less RANKL in comparison to the other groups. The molecular-level regulation of bone metabolism by H_2S is comprised of numerous interdependent signaling pathways and is crucial for bone formation and absorption [38].

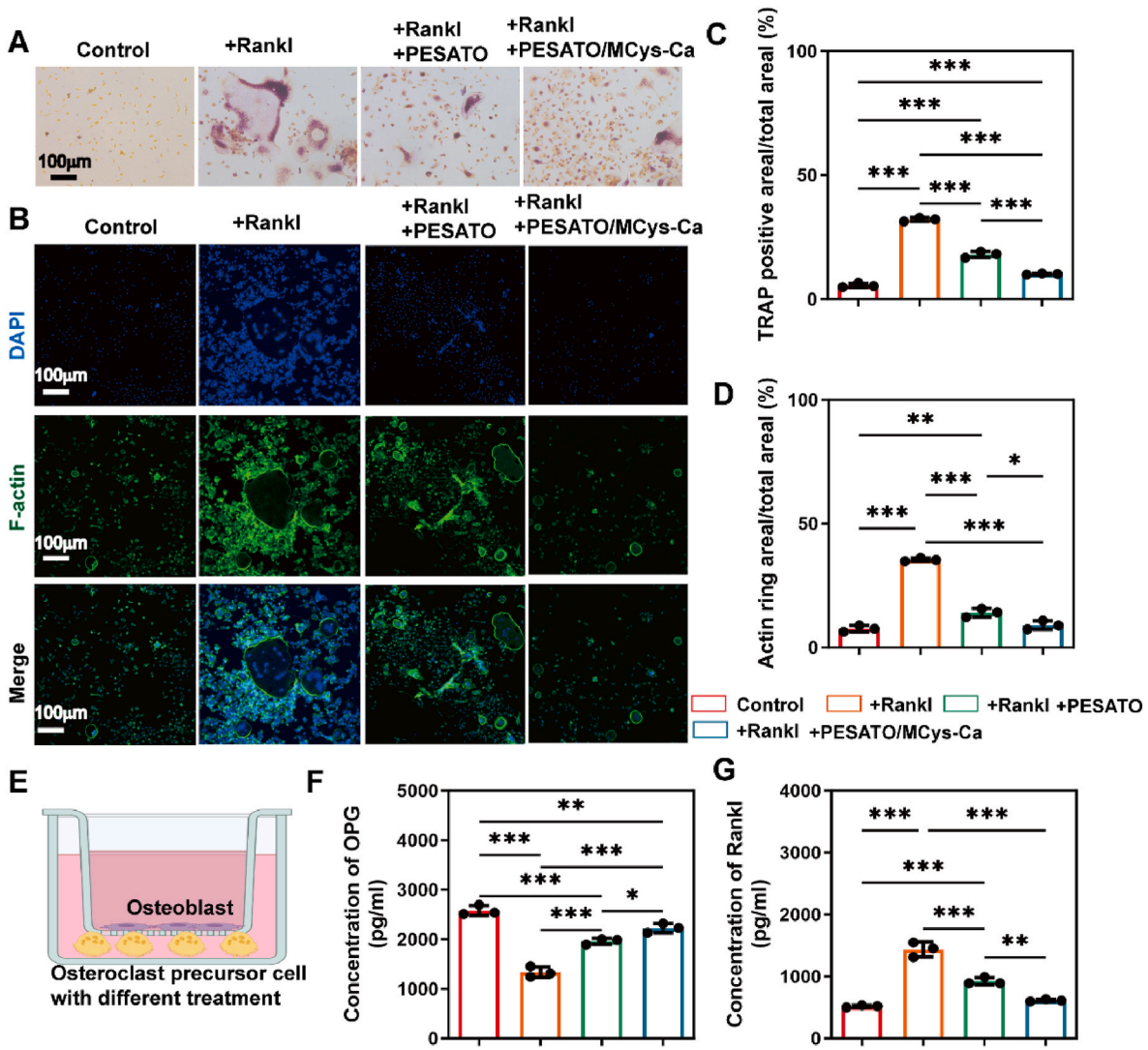

Fig. 4. Composite hydrogels inhibit osteoclastogenesis in vitro. (A) Microscopic images of TRAP staining of cells with different treatments in the lower chamber. Scale bar = 100 μm. (B) Representative images of F-actin staining. Scale bar = 100 μm. (C) Quantitative analysis of the ratio of TRAP-positive areas to total areas. (D) Quantitative analysis of the ratio of F-actin ring areas to total areas. (E) Schematic illustration of pre-osteoblasts and osteoclasts. (F–G) The expression levels of RANKL and OPG in the coculture system after different treatments.

3.5. In vitro evaluation of osteogenic differentiation and tube formation

Biomaterials' biocompatibility is crucial for prospective applications in bone tissue engineering. Using the CCK-8 method, we therefore assessed the cytotoxicity of various hydrogels towards BMSCs and HUVECs. As shown in the results (Fig. 5B–F), the addition of RANKL decreased the OD values relative to the control group. However, the OD values recovered in the hydrogel group, indicating that the hydrogels are non-cytotoxic and can reverse the RANKL-induced decrease in cell viability. Osteogenesis involves BMSCs, which determine both the rate and extent of new bone formation. An ARS staining assay, qPCR, and an ALP activity assay were utilized to examine the capacity of the hydrogels to stimulate the osteogenic differentiation of mesenchymal stem cells in the bone marrow. As a result of its ability to stain calcium deposits, alizarin red can be utilized to ascertain whether osteoblastic differentiation of stem cells has been accomplished. By coculturing cells with various materials, the impact of the materials on the osteogenic differentiation process was investigated, while the addition of RANKL revealed the effect of RANKL on the process. The results presented in Fig. 5A indicate that the addition of RANKL decreased the expression of osteogenic genes (RUNX 2, BMP-2, Col I, ALP, and OCN) but increased the expression of RANKL, in comparison to the control group. Following coculture with the materials, the expression of osteogenic genes was significantly restored by the PESATO/MCys-Ca gel. During the early stages of osteogenesis, the mineralization process of the bone matrix is significantly influenced by the increase in ALP activity. The ALP activity of bone marrow mesenchymal stem cells cultured in various hydrogels for predetermined durations (3 and 14 days) is illustrated in Fig. 5C–D. The ALP activity exhibited by each cohort increased as the culture time extended. The activity of ALP exhibited a notable decline following the introduction of RANKL, as evidenced by the reduced staining of ALP. However, the activity of ALP was reinstated subsequent to coculture with gel, particularly in the PESATO/MCys-Ca group. A comparable trend was noted when ARS staining was applied (Fig. 5E), wherein RANKL impeded calcium deposition throughout the process of osteogenic differentiation, whereas PESATO/MCys-Ca significantly reinstated calcium deposition. These outcomes indicate that the H_2S-releasing gel promotes bone formation more effectively.

Angiogenesis is an essential factor in the process of bone healing. Thus, the capacity of the hydrogel to stimulate angiogenesis was validated via tube formation experiments in HUVECs. As illustrated in Fig. 5G, the angiogenesis capacity of the HUVECs treated with RANKL

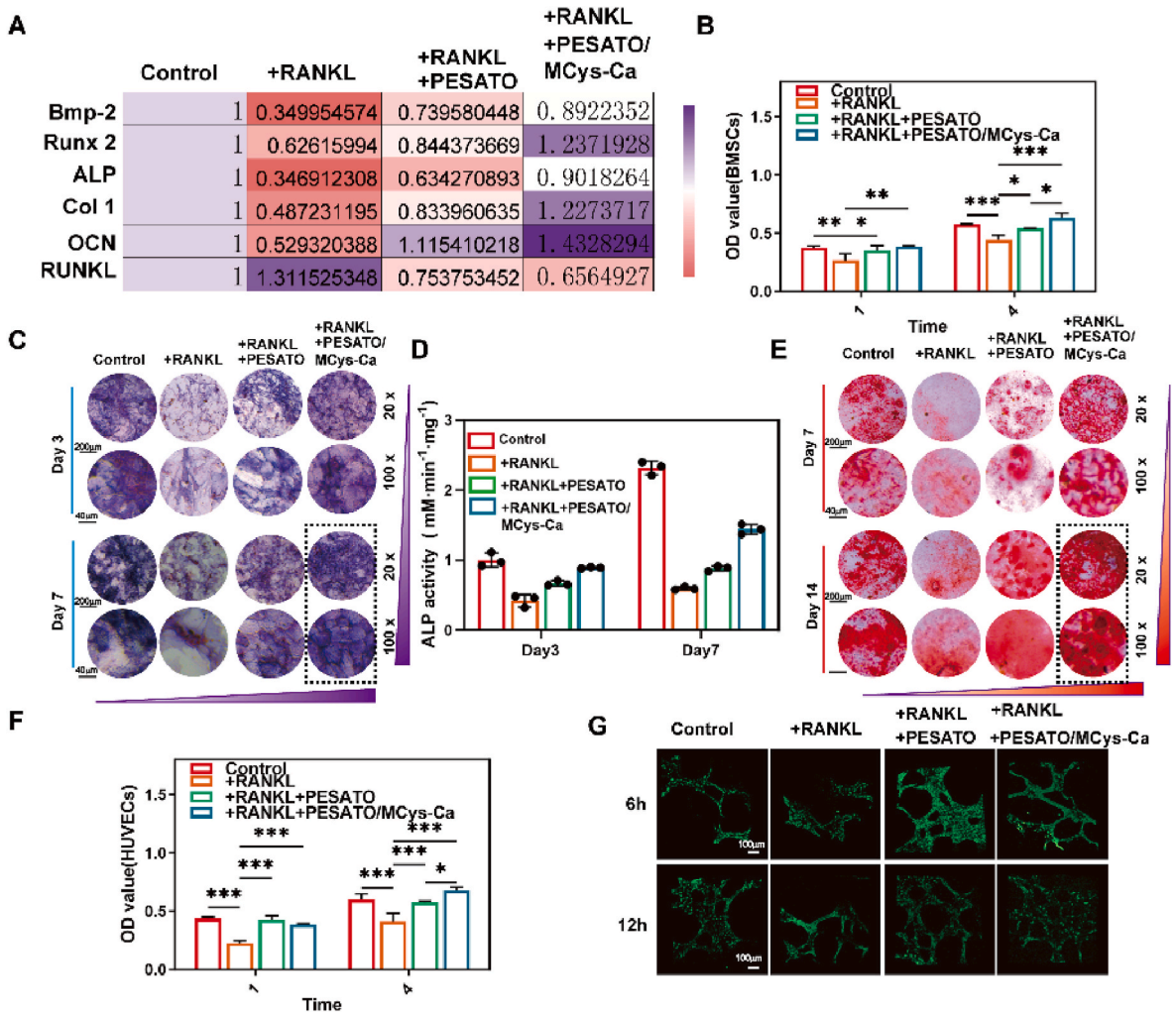

Fig. 5. In vitro osteogenesis of BMSC and tubular formation of HUVEC on composite hydrogel. (A) Heatmap of osteogenic- and osteoclastic-related genes expression of BMSCs under different treatments. (B) BMSCs viability evaluation for 1 and 4 days. (C–D) Qualitative and quantitative results of ALP staining under different treatments. (E) Qualitative results of mineralization staining (ARS straining) under different treatments. (F) HUVECs viability evaluation for 1 and 4 days. (G) The microscopic images of HUVECs tube formation. Scale bars: 50 μm.

was considerably diminished in comparison to the control group. Microscopy images of the formation of HUVEC tubular structures revealed that the hydrogels, specifically the PESATO/MCys-Ca gel, promoted HUVEC tube formation. The findings indicated that the PESATO/MCys-Ca gel exhibited the most potent capacity for angiogenesis. Similar findings to those reported previously indicate that H_2S stimulates the proliferation, migration, and angiogenesis of HUVECs [39,40].

3.6. *In vivo evaluation of osteoporotic bone tissue regeneration*

Due to their complex microenvironment, which is frequently marked by an imbalance of osteoclastogenic activity, elevated ROS levels, and an inflammatory milieu, osteoporotic bone defects are difficult to heal. Treatments that are specialized are required to resolve these complexities. Before evaluation of osteoporotic bone tissue regeneration, the degradation of hydrogels in vivo was evaluated. The results presented in Fig. S1 demonstrate that the PESATO/MCys-Ca hydrogels undergoes gradual degradation over time, with nearly complete degradation occurring within approximately 4 weeks. Furthermore, microscopic analysis reveals significant signs of tissue infiltration after 1 week, accompanied by limited tissue growth; however, there is an increase in tissue invasion observed after 2 weeks. By 3 weeks, the majority of the hydrogel is replaced by tissue. These findings suggest that the PESATO/MCys-Ca hydrogels possess an appropriate degradation rate, making it suitable for tissue repair while facilitating tissue regeneration. In an osteoporotic model, the effectiveness of an injectable hydrogel in response to the discharge of H_2S gas into the ROS microenvironment was evaluated. A bilateral oophorectomy was performed on female rats in order to establish the osteoporosis model. The experimental protocol involving animals is illustrated in detail in Fig. 6A. The OVX group's femoral micro-CT reconstructions (Fig. 6B–C) demonstrated substantial bone loss and a reduced bone volume fraction in the sagittal direction. Histological examinations utilizing H&E and Masson staining provided additional confirmation of diminished bone trabeculae in the OVX group, which signifies the successful establishment of the osteoporosis model.

Following the establishment of the osteoporosis model, a cylindrical defect measuring 4 mm in depth and 3 mm in diameter was drilled into the lateral epicondyle of the OVX rats. At 4 weeks following the procedure, as depicted in Fig. 6B–C, the degree of new bone formation in each defect group varied; however, the untreated control group retained a significant defect area. Repair was accelerated in the hydrogel groups, particularly the PESATO/MCys-Ca group. The presence of substantial defects in the control group 8 weeks post-surgery suggests that the critical defect linked to osteoporosis remained resistant to repair. However, the defects in the PESATO/MCys-Ca group were nearly

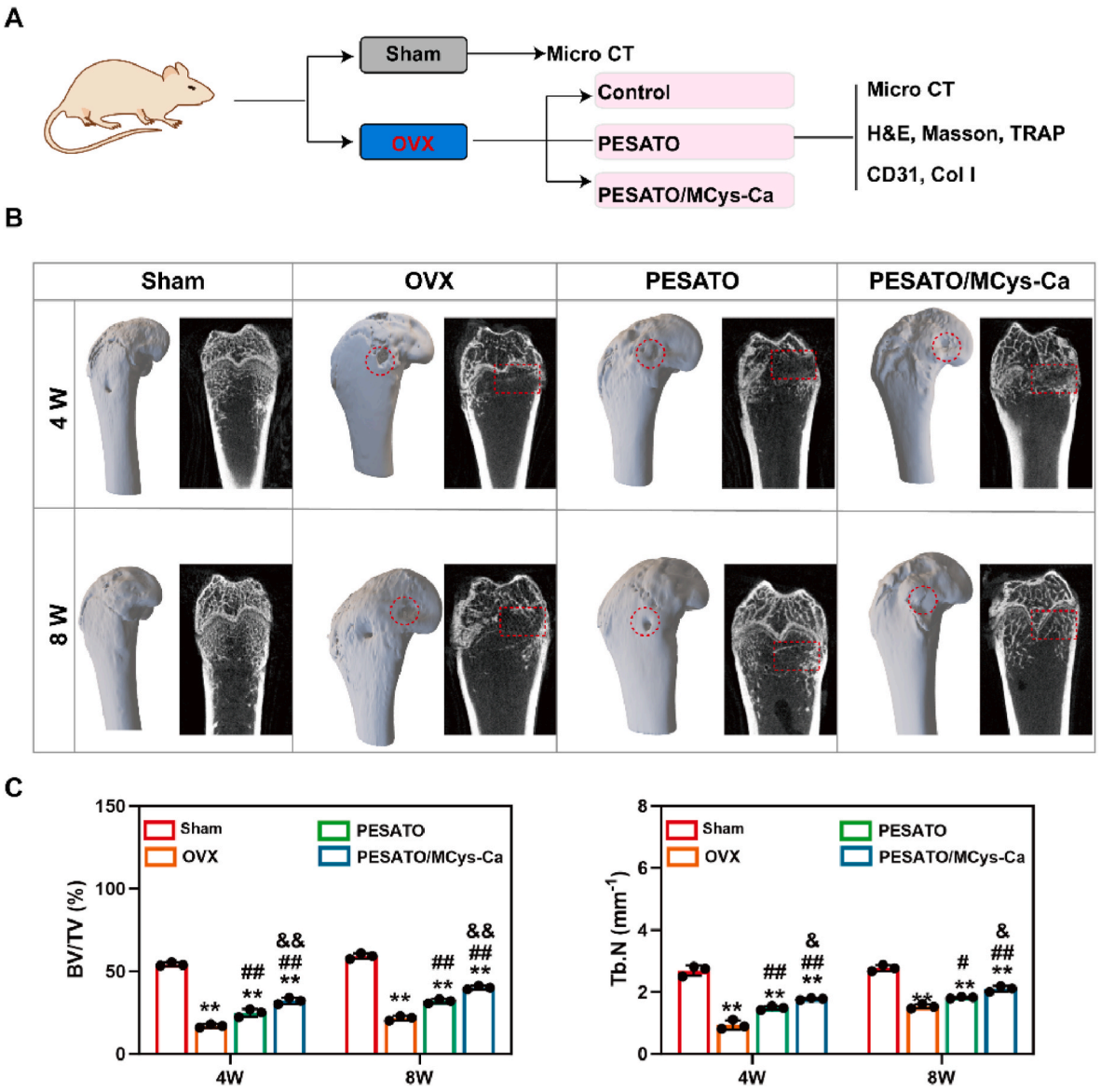

Fig. 6. PESATO/MCys-Ca promoted bone regeneration in OVX rats. (A) Schematic of implantation operation and subsequent steps for in vivo evaluation. (B) Micro-CT 3D reconstructed images and 2D images of the defect site after 4 and 8 weeks of Regeneration. (C–D) Quantification of bone morphological parameters BV/TV and Tb.N.

completely healed, whereas rats in the agglutination group experienced substantial healing. Constantly exhibiting a slightly rough surface, the new bone tissue appeared and felt identical to the surrounding tissue in appearance and color. The quantitative analysis unveiled an analogous pattern. In comparison to the other groups, the PESATO/Cys-Ca group exhibited notably high BV/TV and Tb.N values.

The microstructure of the regenerated tissue was subsequently examined via sectioning and staining of the tissue. The tissue morphology of the bone defects and bone regeneration was additionally examined using H&E and Masson staining, as illustrated in Fig. 7. In comparison to the rats in the other groups, the rats in the PESATO/MCys-Ca group produced the greatest number of bone trabeculae and exhibited the most rapid and optimal regeneration rate 4 weeks after surgery (Fig. 7). Significant defects persisted in the control group 4 and 8 weeks following surgery, suggesting that the bone injury failed to heal gradually. Although there were still visible immature bone bridges and gaps, the quantity of new bone in the PESATO group increased in comparison to the 4-week mark, albeit with limited repair. However, an established and steadfast skeletal structure was observed in the PESATO/MCys-Ca group at the 8-week mark. There was no discernible demarcation between the host bone and the new bone; the host bone had undergone complete integration with the new bone. At four weeks, the PESATO/MCys-Ca group exhibited more active bone remodeling and regeneration processes, as determined by TRAP staining; at eight weeks, neither TRAP staining nor bone maturation were detected. These findings corroborate the micro-CT results, providing further evidence that PESATO/MCys-Ca facilitates the restoration of osteoporotic bone defects.

By employing fluorescence staining for the angiogenic marker CD31/a-SMA and immunohistochemical staining for Col I, vascular regeneration and bone tissue regeneration during the repair process were observed. In contrast to the other groups, the PESATO/MCys-Ca group exhibited elevated levels of Col I and CD31/α-SMA expression at the site of the osteoporotic defect (Fig. 8). This finding suggests that PESATO/MCys-Ca facilitates vascular regeneration and bone repair in osteoporotic defects.

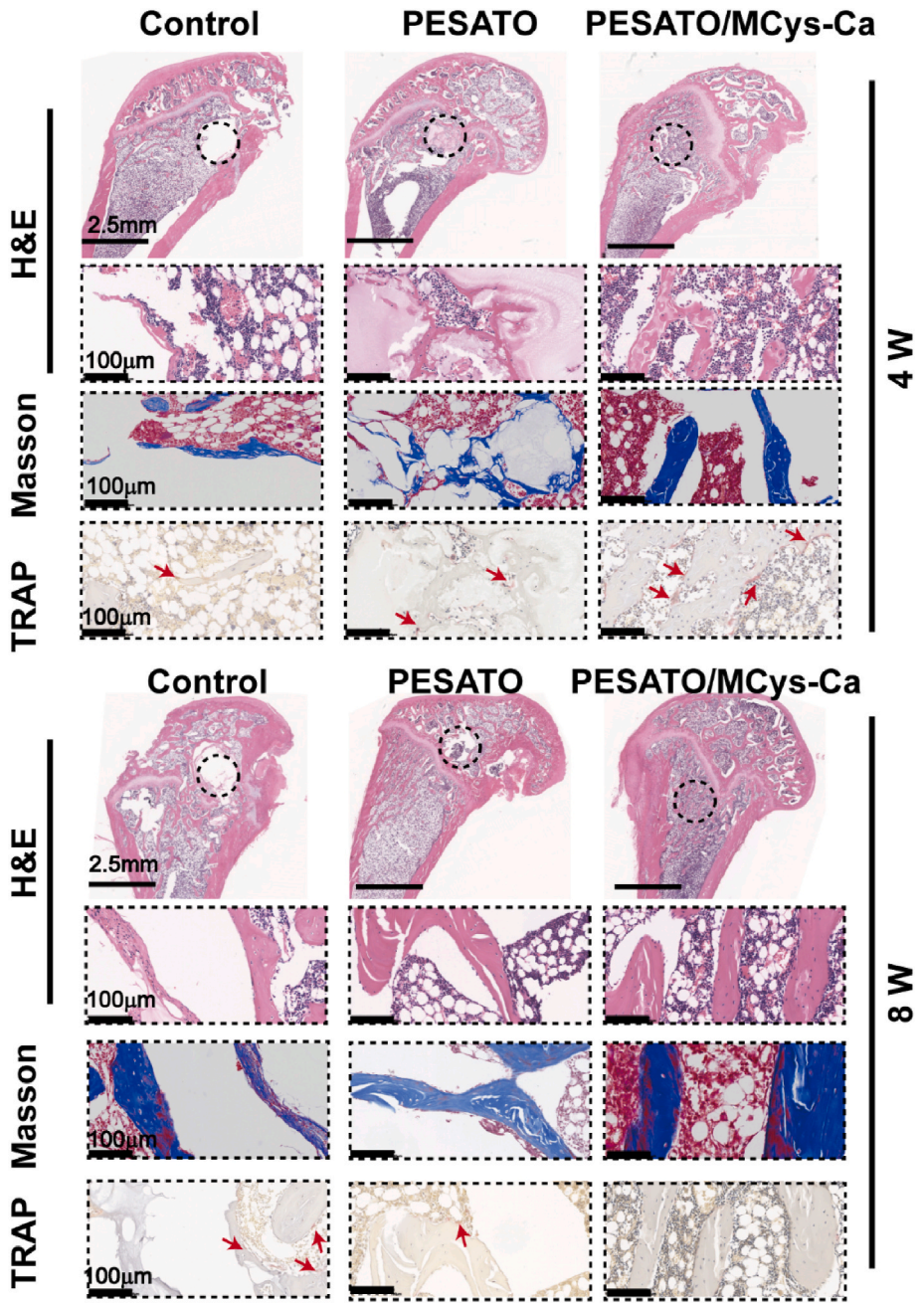

Fig. 7. Representative H&E staining, Masson's trichrome staining and TRAP staining of Femoral bone sections.

4. Conclusion

We successfully developed a double-network injectable hydrogel with the capability to release H_2S. Effective at removing ROS, regulating macrophage polarization, promoting osteogenic differentiation and angiogenesis, inhibiting osteoclast differentiation, and maintaining the osteogenesis/osteoclast balance, this hydrogel possesses excellent mechanical properties. Cys released from the microparticles diffuses into the PESATO gel network when the gel is exposed to the highly oxidative microenvironment of osteoporosis; this causes the gradual and controllable release of H_2S gas, thereby carrying out its function. Several of the hydrogel composite system's biological properties are ideal. The aforementioned findings suggest that the new system exhibits notable benefits in terms of impeding inflammation and fostering bone angiogenesis when applied to osteoporotic bone defects via a multifaceted collaborative strategy. Consequently, this system presents fresh prospects for the clinical management of bone defects.

CRediT authorship contribution statement

Lianghua Jiang: Writing – original draft, Investigation, Formal analysis, Data curation. **Yubin Wu:** Methodology, Data curation. **Zonghan Xu:** Supervision, Funding acquisition, Conceptualization. **Mingzhuang Hou:** Formal analysis. **Shayang Chen:** Data curation. **Chao Cheng:** Visualization. **Dan Hu:** Funding acquisition, Project administration, Validation. **Daming Lu:** Validation, Conceptualization. **Xuesong Zhu:** Writing – original draft, Visualization, Software. **Chong Li:** Writing – review & editing, Validation, Supervision, Resources, Funding acquisition, Conceptualization.

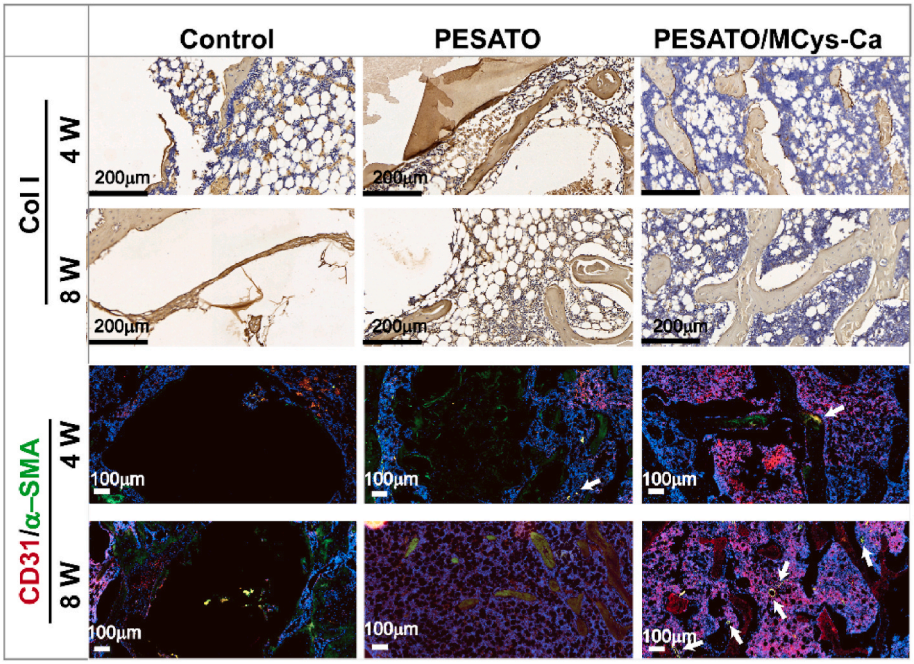

Fig. 8. Immunohistochemical staining in bone defect region by using Col I and CD31/α-SMA antibodies to detect bone regeneration and vascular regeneration.

Declaration of competing interest

The authors declare that they have no known competing financial interests or personal relationships that could have appeared to influence the work reported in this paper.

Acknowledgements

This work was supported by grants from National Natural Science Foundation of China (82072442, 82272494), Natural Science Foundation of Jiangsu Province (BK20240383), Special Funding for Jiangsu Province Science and Technology Plan (Key Research and Development Program for Social Development) (BE2023738), Key Project of the Jiangsu University Medical Education Collaborative Innovation Fund (JDY2022013), Suzhou City Major Disease Multicenter Clinical Research Project (DZXYJ202312), Gusu Health Talent Program (GSWS2022105, GSWS2024182), Major Disease Project of Suzhou Municipal Health Commission (LCZX202110), and Boxi Youth Natural Science Foundation (BXQN2023014).

Appendix A. Supplementary data

Supplementary data to this article can be found online at https://doi.org/10.1016/j.mtbio.2024.101338.

Data availability

Data will be made available on request.

References

[1] R.J. Pignolo, S.F. Law, A. Chandra, Bone aging, cellular senescence, and osteoporosis, JBMR Plus 5 (4) (2021) e10488.
[2] S. Song, Y. Guo, Y. Yang, et al., Advances in pathogenesis and therapeutic strategies for osteoporosis, Pharmacol. Therapeut. 237 (2022) 108168.
[3] E.C. Rodríguez-Merchán, Bone healing materials in the treatment of recalcitrant nonunions and bone defects, Int. J. Mol. Sci. 23 (6) (2022) 3352.
[4] J. Li, L. Li, T. Wu, et al., An injectable thermosensitive hydrogel containing resveratrol and dexamethasone-loaded carbonated hydroxyapatite microspheres for the regeneration of osteoporotic bone defects, Small Methods 8 (1) (2023).
[5] J.E. Compston, M.R. McClung, W.D. Leslie, Osteoporosis, Lancet 393 (10169) (2019) 364–376.
[6] W.J. Boyle, W.S. Simonet, D.L. Lacey, Osteoclast differentiation and activation, Nature 423 (6937) (2003) 337–342.
[7] C. Sobacchi, A. Schulz, F.P. Coxon, et al., Osteopetrosis: genetics, treatment and new insights into osteoclast function, Nat. Rev. Endocrinol. 9 (9) (2013) 522–536.
[8] A. Giuffrè, J.B. Vicente, Hydrogen sulfide biochemistry and interplay with other gaseous mediators in mammalian physiology, Oxid. Med. Cell. Longev. 2018 (2018) 6290931.
[9] Y. Wang, R. Yu, L. Wu, et al., Hydrogen sulfide signaling in regulation of cell behaviors, Nitric Oxide 103 (2020) 9–19.
[10] T.M. Hildebrandt, M.K. Grieshaber, Three enzymatic activities catalyze the oxidation of sulfide to thiosulfate in mammalian and invertebrate mitochondria, FEBS J. 275 (13) (2008) 3352–3361.
[11] Y. Mikami, N. Shibuya, Y. Ogasawara, et al., Hydrogen sulfide is produced by cystathionine γ-lyase at the steady-state low intracellular Ca2+ concentrations, Biochem. Biophys. Res. Commun. 431 (2) (2013) 131–135.
[12] F. Ercole, F.M. Mansfeld, M. Kavallaris, et al., Macromolecular hydrogen sulfide donors trigger spatiotemporally confined changes in cell signaling, Biomacromolecules 17 (1) (2015) 371–383.
[13] Y. Liu, R. Yang, X. Liu, et al., Hydrogen sulfide maintains mesenchymal stem cell function and bone homeostasis via regulation of Ca2+ channel sulfhydration, Cell Stem Cell 15 (1) (2014) 66–78.
[14] J.L. Wallace, R. Wang, Hydrogen sulfide-based therapeutics: exploiting a unique but ubiquitous gasotransmitter, Nat. Rev. Drug Discov. 14 (5) (2015) 329–345.
[15] W. Jiang, F. Hou, Y. Gu, et al., Local bone metabolism balance regulation via double-adhesive hydrogel for fixing orthopedic implants, Bioact. Mater. 12 (2022) 169–184.
[16] R.J. Carrazzone, J.C. Foster, Z. Li, et al., Tuning small molecule release from polymer micelles: varying H2S release through crosslinking in the micelle core, Eur. Polym. J. 141 (2020) 110077.
[17] Y. Huang, Z. Wang, Preparation of composite aerogels based on sodium alginate, and its application in removal of Pb2+and Cu2+from water, Int. J. Biol. Macromol. 107 (2018) 741–747.
[18] E. Boanini, K. Rubini, S. Panzavolta, et al., Chemico-physical characterization of gelatin films modified with oxidized alginate, Acta Biomater. 6 (2) (2010) 383–388.
[19] Y. Zhuang, F. Yu, J. Ma, et al., Enhanced adsorption removal of antibiotics from aqueous solutions by modified alginate/graphene double network porous hydrogel, J. Colloid Interface Sci. 507 (2017) 250–259.
[20] Z-j Shao, X-l Huang, F. Yang, et al., Engineering sodium alginate-based cross-linked beads with high removal ability of toxic metal ions and cationic dyes, Carbohydr. Polym. 187 (2018) 85–93.
[21] S. Thakur, B. Sharma, A. Verma, et al., Recent progress in sodium alginate based sustainable hydrogels for environmental applications, J. Clean. Prod. 198 (2018) 143–159.
[22] Q. Wei, D. Liu, G. Chu, et al., TGF-β1-supplemented decellularized annulus fibrosus matrix hydrogels promote annulus fibrosus repair, Bioact. Mater. 19 (2023) 581–593.
[23] Y.J. Shin, R.T. Shafranek, J.H. Tsui, et al., 3D bioprinting of mechanically tuned bioinks derived from cardiac decellularized extracellular matrix, Acta Biomater. 119 (2021) 75–88.

[24] F. Rong, T. Wang, K. Wang, et al., Core-Cross-linking of polymeric micelles by di-para-substituted S-aroylthiooximes as linkers for controlled H2S release, ACS Macro Lett. 11 (5) (2022) 622–629.
[25] D.M.S.A. Salem, M.A.E. Sallam, T.N.M.A. Youssef, Synthesis of compounds having antimicrobial activity from alginate, Bioorg. Chem. 87 (2019) 103–111.
[26] H. Zhao, J. Huang, Y. Li, et al., ROS-scavenging hydrogel to promote healing of bacteria infected diabetic wounds, Biomaterials 258 (2020) 120286.
[27] J.C. Foster, S.C. Radzinski, X. Zou, et al., H2S-Releasing polymer micelles for studying selective cell toxicity, Mol. Pharm. 14 (4) (2017) 1300–1306.
[28] Y. Zhao, S. Bhushan, C. Yang, et al., Controllable hydrogen sulfide donors and their activity against myocardial ischemia-reperfusion injury, ACS Chem. Biol. 8 (6) (2013) 1283–1290.
[29] X. Zhao, Y. Yang, J. Yu, et al., Injectable hydrogels with high drug loading through B–N coordination and ROS-triggered drug release for efficient treatment of chronic periodontitis in diabetic rats, Biomaterials 282 (2022) 121387.
[30] B. Sun, H. Wang, B. Xiao, et al., Bioactive composite hydrogel with effects of robust promoting osteogenesis and immunomodulation for osteoporotic bone regeneration, Chem. Eng. J. (2023) 476.
[31] J.C. Foster, J.B. Matson, Functionalization of methacrylate polymers with thiooximes: a robust postpolymerization modification reaction and a method for the preparation of H2S-releasing polymers, Macromolecules 47 (15) (2014) 5089–5095.
[32] X. Shen, K. Fang, K.H. Ru Yie, et al., High proportion strontium-doped micro-arc oxidation coatings enhance early osseointegration of titanium in osteoporosis by anti-oxidative stress pathway, Bioact. Mater. 10 (2022) 405–419.
[33] S.C. Manolagas, From estrogen-centric to aging and oxidative stress: a revised perspective of the pathogenesis of osteoporosis, Endocr. Rev. 31 (3) (2010) 266–300.
[34] S. Feng, Y. Zhao, M. Xian, et al., Biological thiols-triggered hydrogen sulfide releasing microfibers for tissue engineering applications, Acta Biomater. 27 (2015) 205–213.
[35] M. Whiteman, S. Le Trionnaire, M. Chopra, et al., Emerging role of hydrogen sulfide in health and disease: critical appraisal of biomarkers and pharmacological tools, Clin. Sci. 121 (11) (2011) 459–488.
[36] T. Nakashima, M. Hayashi, T. Fukunaga, et al., Evidence for osteocyte regulation of bone homeostasis through RANKL expression, Nat. Med. 17 (10) (2011) 1231–1234.
[37] Y. Cui, Y. Guo, L. Kong, et al., A bone-targeted engineered exosome platform delivering siRNA to treat osteoporosis, Bioact. Mater. 10 (2022) 207–221.
[38] Y. Hao, H. Wang, L. Fang, et al., H2S donor and bone metabolism, Front. Pharmacol. 12 (2021).
[39] A. Longchamp, K. Kaur, D. Macabrey, et al., Hydrogen sulfide-releasing peptide hydrogel limits the development of intimal hyperplasia in human vein segments, Acta Biomater. 97 (2019) 374–384.
[40] D. Céline, M. Laurence, A. Florian, et al., Atorvastatin-loaded hydrogel affects the smooth muscle cells of human veins, J. Pharmacol. Exp. Therapeut. 347 (3) (2013) 574.